



Research paper

Nanostructure-loaded mesoporous silica for controlled release of coumarin derivatives: A novel testing of the hyperthermia effect

Ahmed S. Al-Kady^a, M. Gaber^a, Mohamed M. Hussein^b, El-Zeiny M. Ebeid^{a,c,*}

^a Chemistry Department, Tanta University, Tanta, Egypt

^b Faculty of Pharmacy, Cairo University, Cairo, Egypt

^c Misr University for Science and Technology (MUST), 6th October City, Egypt

ARTICLE INFO

Article history:

Received 8 June 2010

Accepted in revised form 19 October 2010

Available online 23 October 2010

Keywords:

Mesoporous silica

Hydroxyapatite nanocomposites

Gold nanorods

Coumarin thiourea

Controlled release

Hyperthermia effect

ABSTRACT

The synthesis of three types of mesoporous materials is reported: pure mesoporous silica (MCM-41), a nanocomposite of mesoporous silica with hydroxyapatite (MCM-41-HA) and mesoporous silica/gold nanorods nanocomposite (MCM-41-GNRs). The mesoporous materials were characterized by X-ray diffraction, N₂ adsorption isotherms, FTIR spectroscopy, transmission electron microscopy, and scanning electron microscopy. The samples were loaded with coumarin thiourea derivatives (I–IV) having functional groups of varying sizes and the in vitro release assays were monitored, and the release behavior was investigated as a function of soaking time in simulated body fluid. Two release stages were obtained in MCM-41, MCM-41-HA and MCM-41-GNRs loaded samples with the early release stages accounting for about 30% of loaded derivatives. These early release stages are characterized by Higuchi rate constant values nearly twice the values associated with the second release stages. The influence of substituent size on the release rate constants was explained in terms of sorption sites and hydrogen bonding with silanol groups on silicates. The release of coumarin derivatives loaded on MCM-41, MCM-41-HA and MCM-41-GNRs occurs over remarkably long time of the order of about 260 h with faster release rates in loaded MCM-41 and MCM-41-GNRs samples compared with MCM-41-HA ones. The role of hyperthermia effect in enhancing release rates was investigated by subjecting loaded MCM-41-GNRs to near infrared (NIR) radiation at 800 nm. This would be of significance in targeted drug release using hyperthermia effect. Unlike hydroxyl apatite, loading MCM-41 with gold nanorods does not affect the release kinetics. Only when these samples are irradiated with NIR photons, does the release occur with enhanced rates. This property could be valuable in selected targeting of drugs.

© 2010 Elsevier B.V. All rights reserved.

1. Introduction

The administration of drugs by a drug delivery system provides advantages over conventional drug therapies because the drug is delivered locally rather than systemically. This minimizes harmful side effects [1]. The entire drug dose needed for a desired period is administered at one time and released in a controlled manner. Other potential advantages include drug targeting, improved compliance and comfort [2]. Numerous systems have been studied for controlled drug delivery, such as biodegradable polymers [3], hydroxyapatite (HA) [4–6], calcium phosphate cement [7–9], xerogels [10,11], hydrogels [12,13] mesoporous silica [14] and others.

Abbreviations: MCM-41, Mesoporous silica; MCM-41-HA, Mesoporous silica/hydroxyapatite nanocomposite; MCM-41-GNRs, Mesoporous silica/gold nanorods nanocomposite.

* Corresponding author. Chemistry Department, Faculty of Science, Tanta University, Tanta, Egypt. Tel.: +20 2 403318302.

E-mail address: drzeiny@yahoo.com (El-Zeiny M. Ebeid).

Mesoporous materials show ordered arrangements of channels and cavities of different geometries built up from SiO₂ units [15]. These materials exhibit variable pore size (2–50 nm), high surface areas (ca. 1000 m²/g), high pore volume (ca. 1 cm³/g) and homogeneous nanostructures which can be tailored by varying the synthesis procedure [16]. The pore walls have high surface density of silanol groups (Si–OH) that could be reactive toward appropriate guest molecules [17].

Siliceous mesoporous materials have the advantage of being biocompatible and degradable in aqueous solutions, and thus problems related to the removal of the material after use can be avoided.

Since 2001, when MCM-41 was purposed for the first time as controlled delivery system [18], much research efforts have been devoted to tailor the chemical properties of mesoporous carriers at the nanometer scale to achieve a better control over loading and release of molecules. The mesoporous carrier is selected according to the features of the guest molecule and the targeted application. Therefore, different guest molecules have been

successfully confined into mesoporous silicas. Some of these molecules are drugs [18–25]. Other guest molecules consisted of biologically active species, such as proteins, e.g. bovine serum albumin (BSA) [26] and certain amino acids [27]. The textural properties (i.e., pore diameter, surface area and pore volume) of mesoporous materials are key factors that govern molecules adsorption and release [28]. Moreover, functionalization of silica walls using different organic groups has been revealed as the main strategy to modulate molecule loading and release.

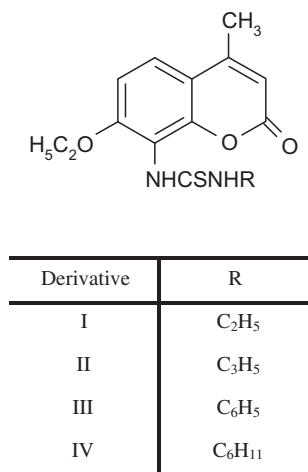
Nanoparticles derived from gold provide an attractive system for diagnostic and therapeutic applications owing to their ease of preparation, ready bioconjugation, good biocompatibility, and unique optical properties [29–31].

In particular, gold nanorods (GNRs) are important metal nanomaterial with distinctive shape-dependent optical properties. Especially, they possess two distinct plasmon bands, one associated with the transverse mode and the other with the longitudinal modes. These properties suggest several advantages of GNRs for the applications not only in biological sensing [32] and imaging [33] but more importantly, they are potential candidates for localized photothermal therapy because they mediate strong plasmon-induced surface heat flux upon absorption of near infrared light [34–37].

Although most of the synthetic methods used for the preparation of metal nanorods suffered from limitations, either in the amount of material [38] or in the yield of nanorods, when compared to nanospheres [39], Nikoobakht and El-Sayed recently reported a variation of the so-called seed-mediated method [40] that affords the synthesis of relatively large amounts of nanorods with very little contamination by nanospheres and variable aspect ratio.

Coumarin derivatives possess a wide range of applications as anticoagulants [41], antitumor [42], photosensitizers [43], anti-HIV [44], antimicrobial [45] and anti-inflammatory agents [46]. Coumarin derivatives have been linked to other molecules in gene expression studies [47] as well as in salmonella detection [48]. Coumarin derivatives are also currently used as fluorogenic dyes in proteomics [49].

In the present communication, we report the application of mesoporous silicate, mesoporous silicate coating gold nanorods and mesoporous silicates loaded by apatite nanostructures as carriers for coumarin thiourea derivatives (I–IV) linked to functional groups of varying sizes in an effort to correlate group size and release rate constants. The advantage of using mesoporous silicates as carriers of the present coumarin derivatives is the remarkably long time-scale of release (Scheme 1).



Scheme 1.

Loading mesoporous silicates with gold nanorods offers a novel method of enhanced release based on hyperthermia effect. Plasmon-resonant gold nanorods are highly effective at transducing NIR light into heat leading to localized hyperthermia. Hyperthermia is currently under consideration as a noninvasive approach to cancer therapy, in which biological tissues are exposed to higher than normal temperatures to promote the selective destruction of abnormal cells [37]. Our present approach offers a dual action in which hyperthermia effect can produce severe blebbing in cell membranes, and render them permeable to chemical agents. The other simultaneous effect is the enhanced release of drugs loaded on mesoporous silicates. The biosafety of metallic gold is well known, and they have been used in vivo since the 1950s and recently the noncytotoxicity of gold nanoparticles in human cells has been studied in detail by Wyatt et al. [50].

2. Materials and methods

2.1. Materials

Analytical grade tetraethyloxysilane (TEOS) was purchased from Merck. Cetyltrimethyl ammonium bromide (CTAB), sodium hydroxide (NaOH), dipotassiumhydrogenphosphate (K₂HPO₄), sodium chloride (NaCl), potassium chloride (KCl), calcium chloride dihydrate (CaCl₂·2H₂O), sodium sulphate decahydrate (Na₂SO₄·10H₂O), magnesium chloride hexahydrate (MgCl₂·6H₂O) and hydrochloric acid (HCl) were purchased from Fluka. Tetrachloroauric acid (HAuCl₄·3H₂O), cetyltrimethyl ammonium bromide (CTAB), benzyldimethylhexadecyl-ammonium chloride (BDAC), ascorbic acid, sodium borohydride, silver nitrate, tris(hydroxymethyl)aminomethane (Tris buffer), acetonitrile (ACN), tetramethyl ammonium hydroxide pentahydrate (TMAOH) and calcium chloride (CaCl₂) were purchased from Aldrich. All materials were used as received without further purification.

2.2. Synthesis of coumarin derivatives (I–IV)

Coumarin derivatives (I–IV) were prepared starting with 4-methyl-7-hydroxy-8-nitrocoumarin [51]. A mixture of 4-methyl-7-hydroxy-8-nitrocoumarin (22.1 g; 0.1 mol) was refluxed with anhydrous potassium carbonate (27.6 g; 0.2 mol) and ethyl iodide (23.6 ml; 0.4 mol) in dry acetone (300 ml) with continuous stirring for 15 h then cooled, filtered and washed with acetone. The combined filtrate and wash was concentrated, the separated solid was filtered and washed with water then crystallized from ethanol to give 7-ethoxy-4-methyl-8-nitrocoumarin of m.p. 179 °C (90%). A suspension of the nitrocoumarin (10 g), stannous chloride dihydrate (40 g), in 95% ethyl alcohol (40 ml) and HCl (120 ml) was boiled for 5 min to give a clear solution. The separated crystals obtained after cooling were filtered, suspended in water and treated with NaHCO₃. The yellow solid separated was filtered, extracted with hot isopropanol, concentrated in vacuum, and the separated shiny yellow crystals were filtered and recrystallized from ethanol to give 8-Amino-7-ethoxy-4-methyl-coumarin: 7.4 g of m.p. 127–8 °C (80%).

8-Alkylthiourido 7-ethoxy-4-methyl-coumarins (I–IV) were obtained by heating a solution of the amine (2.2 g; 0.01 mol in 20 ml ethanol) with the appropriate isothiocyanate derivative (0.01 mol) in alcohol with stirring for 6 h. The product was concentrated and filtered. The separated solid was recrystallized from ethanol to give the desired compound.

2.3. Synthesis of mesoporous silica (MCM-41)

First, 0.46 g NaOH was dissolved into 120 ml deionized H₂O with stirring. After the solution becomes clear, 1.4 g CTAB was

dissolved completely, 5.6 ml TEOS was poured into the above solution under vigorous stirring. Stirring was continued for 24 h, then the mixture was heated at 80 °C for 48 h. The mixture was filtered to obtain solid silica particles then dried at 100 °C for 6 h, and the surfactant was removed by calcination at 550 °C for 5 h.

2.4. Synthesis of mesoporous silica/apatite nanocomposite (MCM-41-HA)

The synthesis of nanocomposites was initiated with the preparation of two different solutions of (2.01 g/60 ml) $\text{CaCl}_2 \cdot \text{H}_2\text{O}$ and (2.71 g/60 ml) K_2HPO_4 in deionized water. Cationic surfactant (CTAB) 2.4 g was dissolved in the solution containing phosphate under constant stirring. The pH at 12 was controlled with TMAOH. The mixture was kept under constant stirring in a closed container at 30 °C. CaCl_2 solution was added, and the agitation was kept for 30 h. After this, 5 ml TEOS was added under agitation, and the final mixture was heated for 24 h at 100 °C under static conditions. The mixture was filtered to obtain the silica/apatite nanocomposite that was dried at 100 °C for 6 h, and the surfactant was removed by calcination at 550 °C for 5 h.

2.5. Synthesis of gold nanorods (GNRs)

Seed-mediated growth was performed at 25 °C from freshly prepared aqueous solutions following methods of Nikoobakht and El-Sayed [40]. Briefly, 2.5 ml of 1.0 mM HAuCl_4 was added to 5.0 ml of 0.2 M cetyltrimethylammonium bromide (CTAB). Six hundred microliters of ice-cold 10 mM NaBH_4 was added to the stirred solution and allowed to react for several minutes, forming the pale brown gold seed solution. Next, 100.0 ml of 1.0 mM HAuCl_4 was added to 100.0 ml of a solution of 0.12 M CTAB and 0.15 M benzyltrimethylhexadecylammonium chloride (BDAC), and 4.5 ml of 4.0 mM AgNO_3 . Approximately 1.4 ml of 78.8 mM ascorbic acid was added, followed by gentle mixing to form the transparent growth solution. One hundred sixty microliters of the seed solution was added to the unstirred growth solution and allowed to react for 2 h. Nanorods synthesized by this method yield pure nanorods of approximately 12 nm in width and 50 nm length (4.0 aspect ratio), with a longitudinal plasmon absorption maximum at 800 nm.

2.6. Synthesis of mesoporous silica coating gold nanorods (MCM-41-GNRs)

Silica coating of gold nanorods were prepared as follows: 1.38 g NaOH were dissolved into 120 ml H_2O with stirring. After the solution becomes clear, 4.2 g CTAB was dissolved completely. Then gold nanorods solution was added, 16.8 ml TEOS was poured into the above solution under vigorous stirring. Stirring was continued for 24 h, then the mixture was heated at 80 °C for 48 h. The mixture was filtered to obtain the silica coating of gold nanorods solid particle, and the surfactant was removed by calcination at 550 °C for 5 h.

2.7. Preparation of simulated body fluid (SBF)

An acellular simulated body fluid that has inorganic ion concentrations similar to those of human extracellular fluid was developed [52] in order to reproduce formation of apatite on bioactive materials in vitro. This fluid can be used for not only evaluation of bioactivity of artificial materials in vitro, but also coating of apatite on various materials under biomimetic conditions. SBF solution was prepared by dissolving appropriate quantities of reagent grade 8.2187 g NaCl, 0.2260 g KCl, 0.3860 g $\text{CaCl}_2 \cdot 2\text{H}_2\text{O}$, 0.3508 g NaHCO_3 , 0.3337 g $\text{K}_2\text{HPO}_4 \cdot 3\text{H}_2\text{O}$, 0.1697 g $\text{Na}_2\text{SO}_4 \cdot 10\text{H}_2\text{O}$,

0.3366 g $\text{MgCl}_2 \cdot 6\text{H}_2\text{O}$ and 50 mM Tris buffer in 1 l distilled water. And 45 mM HCl was used to maintain pH of the solution at 7.4 similar to blood plasma pH (osmolarity = 364.3 mosm/l).

2.8. Coumarin derivatives (I–IV) loading

To evaluate the performance of the MCM-41, MCM-41-HA and MCM-41-GNRs for hosting therapeutic systems, the initial calcined powders (MCM-41, MCM-41-HA and MCM-41-GNRs) were compressed into 0.25 g disks by uniaxial pressure of 1.5 MPa. The disks were soaked in saturated solutions of coumarin thiourea derivatives (I–IV) (6 mg/ml acetonitrile) for 4 days at room temperature.

2.9. Coumarin derivatives (I–IV) release from MCM-41 and MCM-41-HA

The in vitro release study of coumarin thiourea derivatives (I–IV) from MCM-41 and MCM-41-HA were performed by soaking MCM-41 or MCM-41-HA disks in 30 ml of simulated body fluid (SBF). The temperature was maintained constant (37 °C), and the solutions were continually stirred. UV spectrometry was used for monitoring the amount of drug release as a function of time. The concentrations of coumarin thiourea derivatives (I–IV) in SBF were found from the absorbance at 320 nm.

2.10. Coumarin derivative (I) release from MCM-41-GNRs

The in vitro release study of coumarin thiourea derivative (I) from MCM-41-GNRs was performed by soaking two disks of MCM-41-GNRs in two different 30 ml of simulated body fluid (SBF). One of them was irradiated at 800 nm during the release study, while the other was not.

2.11. X-ray diffraction studies

X-ray diffraction analysis was carried out using a Philips PW 1390 X-ray diffractometer using copper target with nickel filter. Each sample was subjected to X-ray analysis under working conditions of 40 kV and 20 mA. All the diffractograms were investigated in the 2θ values in the range of 5–70° at room temperature.

2.12. Fourier transform infrared spectroscopy (FTIR) studies

Fourier transform infrared spectroscopy was recorded on a Perkin–Elmer 1430 spectrophotometer in the range of 4000–400 cm^{-1} . The FTIR spectra were recorded at room temperature in KBr pellets.

2.13. Nitrogen adsorption analysis

Specific surface area and pore size distribution were determined by N_2 adsorption using the BJH method in an Autosorb – Quantachrome NOVA 1200.

2.14. Scanning electron microscopy (SEM) and transmission electron microscopy (TEM) studies

The particle size and morphology were analyzed by scanning electron microscopy (SEM), JSM-5200LV. The copper disc was pasted with carbon tape, and the sample was dispersed over the tape. The disc was coated with gold in an ionization chamber. Transmission electron microscopy (TEM) was performed using JEOL-JEM 1230 electron microscope, operating at an accelerating voltage of 120 kV. Samples for TEM were prepared by depositing a drop of either the nanorod colloid or the suspension of a ground

piece of mesoporous silica in ethanol, on a carbon-coated TEM copper grid and left to evaporate at room temperature.

2.15. Spectrophotometric studies

The releasing of coumarin thiourea derivatives at different time intervals was measured at $\lambda = 320$ nm using a Shimadzu UV-160A spectrophotometer connected to a Haake ultrathermostat.

2.16. Laser diode studies

Laser irradiation for hyperthermia effect was carried out at 807 nm using a diode laser driver Model (LDD-9), ATC semiconductor devices. The laser power at the sample position was 2.7 W.

3. Results and discussion

3.1. Characterization studies

Fig. 1a displays TEM observation of MCM-41 particles. MCM-41 silica material was obtained as small spherical particles with a diameter of about 1 μm . The TEM image (Fig. 1b) shows the characteristic hexagonal arrangement of uniform pores and unidirectional canals for the MCM-41 sample. SEM imaging shows the growth of crystalline particles, and the surface was completely covered with them (Fig. 2a). A similar image was reported by Sousa et al. [17]. The template-guided one-pot synthesis method allows a fairly homogenous distribution of the mesoporous silica throughout the apatite crystal surface. This is demonstrated in the TEM image in Fig. 2b. The TEM image of GNRs (Fig. 3a) shows that the GNRs have an average aspect ratio of 4.0 with length of ca. 50 nm and width of ca. 12 nm. The morphology of the MCM-41-GNRs sample is shown in Fig. 3b. It is clear that the nanorods are well separated and homogeneously distributed in its interior. This separation allows to basically maintain the optical properties of individual nanorods within the final mesoporous structure.

Fig. 4 shows surface plasmon absorption spectrum of GNRs. The strong long wavelength band in the near infrared region around 800 nm is due to the longitudinal oscillation of electrons and the weak short wavelength band in the visible region around 520 nm is due to the transverse electronic oscillation.

Fig. 5 shows the XRD patterns for MCM-41, MCM-41-HA and MCM-41-GNRs. MCM-41 is an amorphous material (Fig. 5a). The XRD pattern of the nanocomposite (Fig. 5b) presents, beyond a typical reflection that is characteristic for the hydroxyapatite (HA) phase, an amorphous region between 10° and 35° , which indicates the presence of two phases in the formed product. These are identified as the nanocomposite formed by HA and amorphous silica [53]. The XRD pattern of MCM-41-GNRs (Fig. 5c) presents the XRD peak at $2\theta = 22^\circ$ corresponding to amorphous mesoporous silica host and those at $2\theta = 38^\circ, 44^\circ, 65^\circ, 78^\circ$ and 82° corresponding to metallic gold [54].

Fig. 6 shows the nitrogen isotherms of MCM-41, MCM-41-HA and MCM-41-GNRs. The nitrogen adsorption-desorption isotherms of MCM-41 and MCM-41-GNRs (Fig. 6a and c) materials exhibit a reversible type IV in the IUPAC classification of mesoporous materials [55]. The leap in the curve can be due to the capillary condensation of nitrogen in the channels of the mesoporous [56]. The data calculated from the curves indicate that the MCM-41 possess a narrow pore size distribution with an average pore size of about 3.38 nm, characteristic of mesoporous materials with well ordered structure. However, MCM-41-HA (Fig. 6b) shows the type-H3 hysteresis loop [17], which presents a broader pore size distribution. The narrow hysteresis loops appeared in the nitrogen adsorption-desorption isotherms indicated that the pore system is

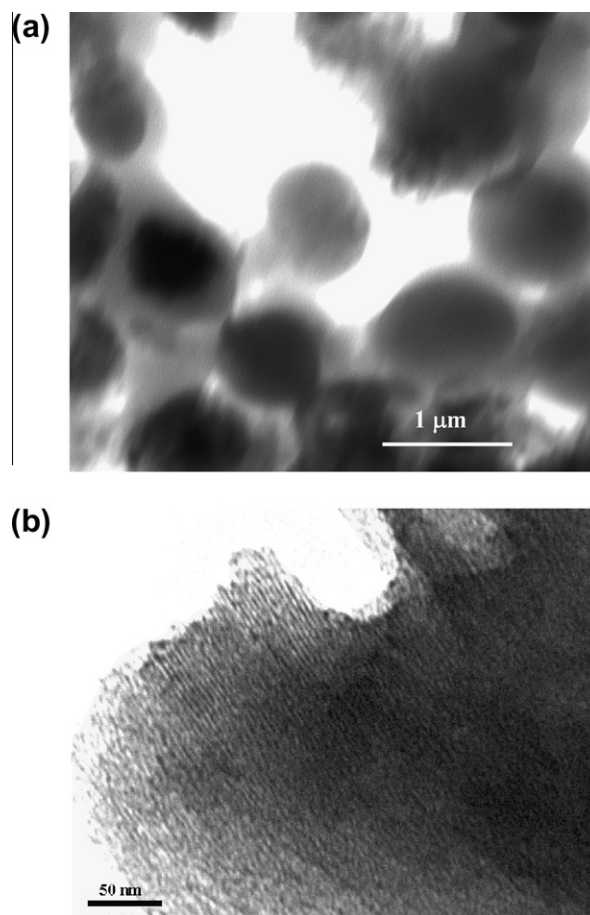


Fig. 1. TEM photographs of (a) MCM-41 particles and (b) MCM-41 (enlarged).

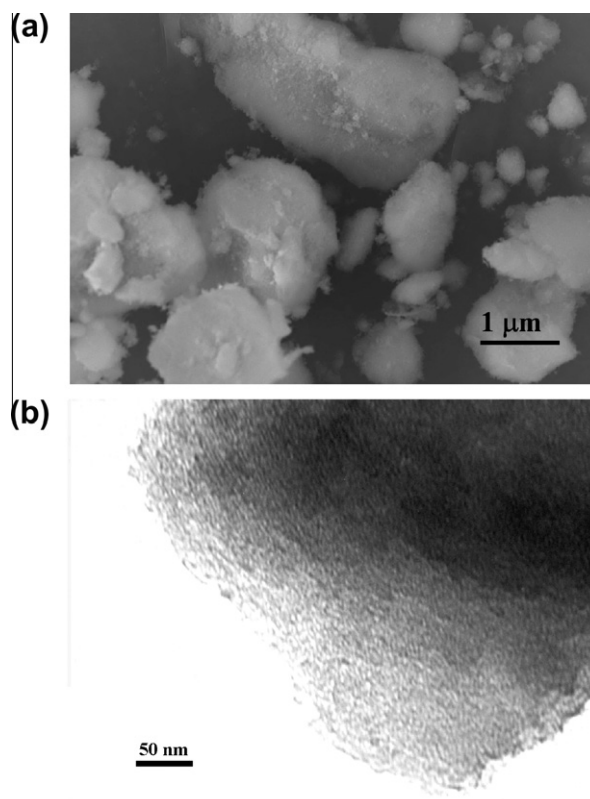


Fig. 2. Photographs of MCM-41-HA particles using: (a) SEM and (b) TEM.

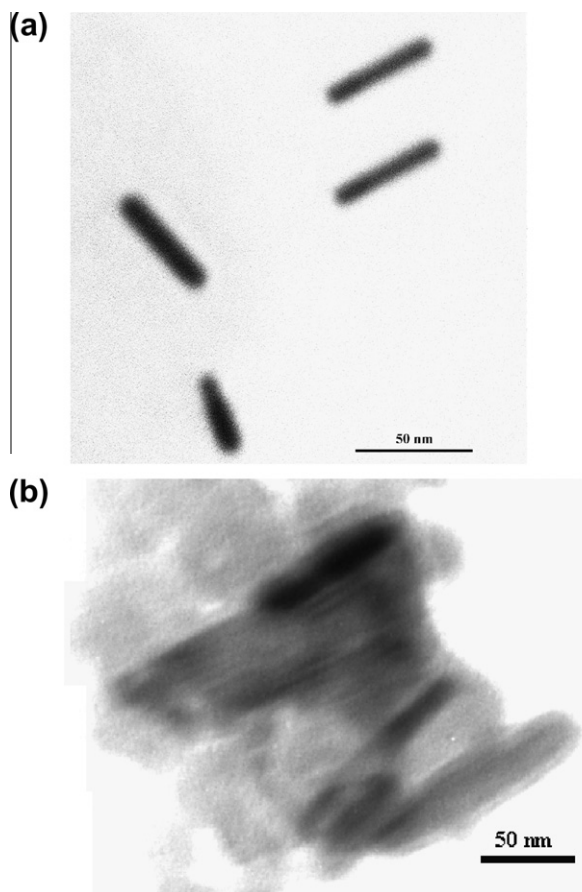


Fig. 3. TEM photographs of (a) GNRs with average aspect ratio of 4.0 and (b) MCM-41 loaded with gold nanorods (MCM-41-GNRs).

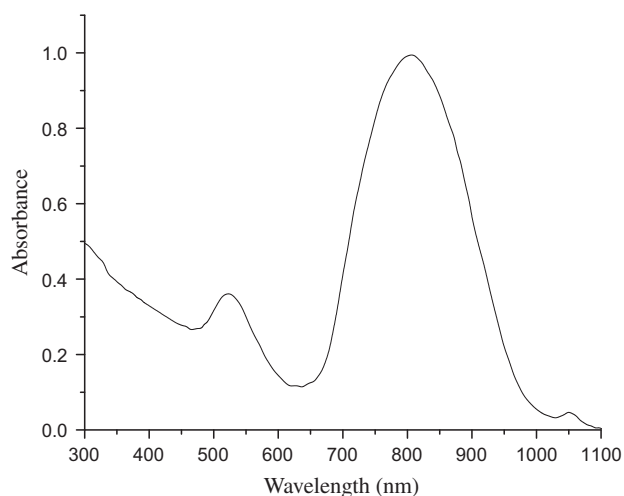


Fig. 4. Surface plasmon absorption spectrum of GNRs.

mainly composed of mesopores with limited sizes and numbers. Table 1 summarizes these results and shows the different pore diameters (D_p), specific surface areas (S_{BET}), and pore volumes (V_p) for the samples. The pore diameter increases from 3.38 nm for pure MCM-41 to 6.08 nm with the introduction of hydroxyapatite in the structure of the MCM-41-HA. MCM-41 surface area of ca. 1011.3 m^2/g decreased to ca. 133.91 m^2/g for MCM-41-HA samples. These differences suggest that the crystal growth of hydroxyapatite blocks the available spaces of the mesoporous silica and are

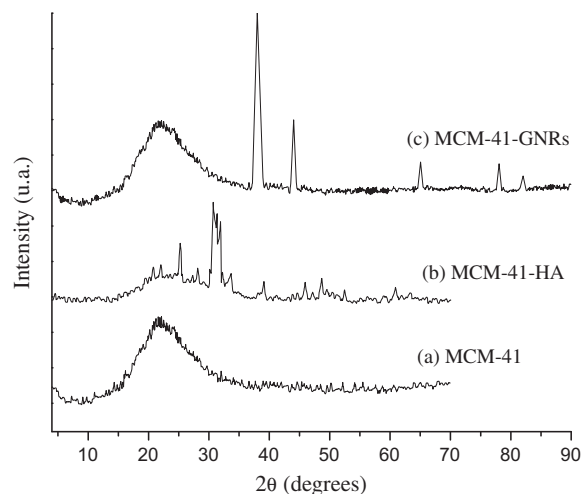


Fig. 5. XRD for: (a) MCM-41, (b) MCM-41-HA and (c) MCM-41-GNRs.

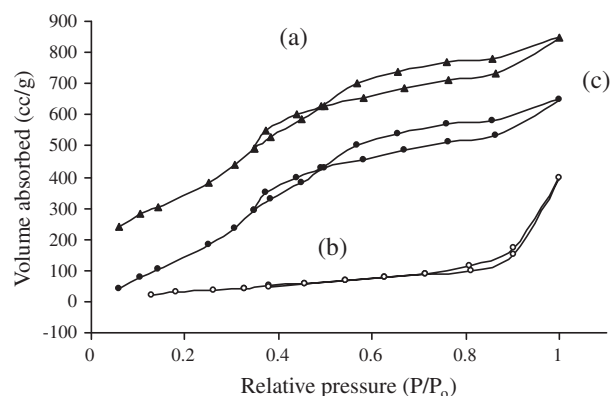


Fig. 6. Nitrogen adsorption and desorption isotherms of (▲) MCM-41, (○) MCM-41-HA and (●) MCM-41-GNRs.

responsible for the increased average diameter of pores. This indicates that the original mesoporous MCM-41 are filled by HA nanocrystals.

FTIR spectra of MCM-41, MCM-41-HA, MCM-41-GNRs and loaded matrices with coumarin thiourea (I–IV) were recorded. Fig. 7A and B shows the comparison of FTIR spectra that exhibit different absorption bands. The main peaks in Fig. 7A(a) are characteristic of the mesoporous silica network. The band at 3400 cm^{-1} is assigned to silanol groups linked to molecular water through hydrogen bonds with internal Si–OH groups. The broad band at 1655 cm^{-1} is assigned to absorbed molecular water. Other bands are as follows: 1100 cm^{-1} for Si–O–Si dissymmetry stretching vibration, 960 cm^{-1} for Si–O–H deformation, 805 cm^{-1} for Si–O–Si symmetry stretching vibration and 460 cm^{-1} for Si–O–Si bending vibration [57]. The strong bands of OH (3400 cm^{-1}) and H_2O (1655 cm^{-1}) indicate that a large number of OH groups and H_2O molecules are present on the surface, which plays an important role in bonding between mesoporous silica and coumarin

Table 1
Nitrogen adsorption–desorption isotherm data of MCM-41, MCM-41-HA and MCM-41-GNRs samples.

Sample	V_p (cm^3/g)	D_p (nm)	S_{BET} (m^2/g)
MCM-41	1.177	3.38	1011.3
MCM-41-HA	0.204	6.08	133.9
MCM-41-GNRs	0.95	3.10	815.0

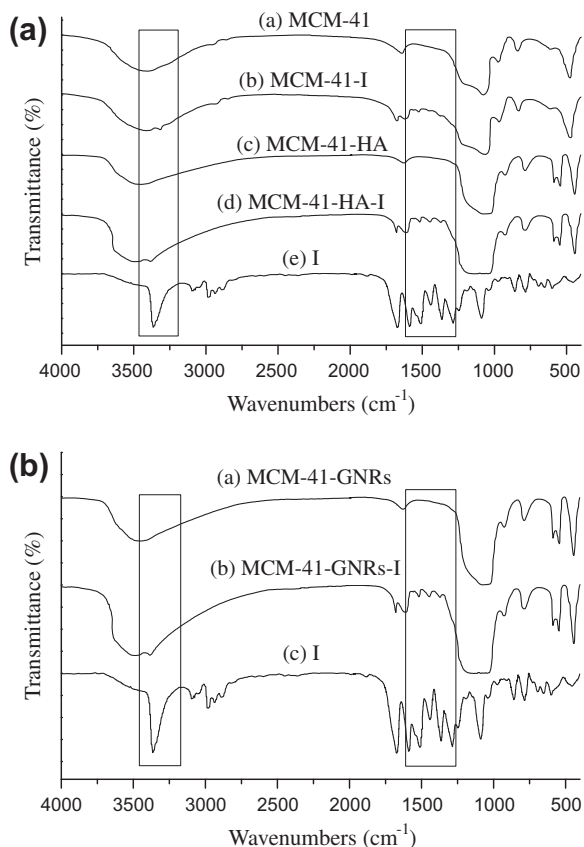


Fig. 7. (A) FTIR spectra of (a) pure MCM-41, (b) MCM-41-sample I, (c) MCM-41-HA, (d) MCM-41-HA-sample I, and (e) Sample I. (B) FTIR spectra of (a) MCM-41-GNRs, (b) MCM-41-GNRs-sample I and (c) sample I.

thiourea (I–IV) molecules. In the spectrum of MCM-41-HA, Fig. 7A(c), some stretching bands that are characteristic of hydroxyapatite pattern are observed. The absorption bands at 563, 603 and 630 cm^{-1} were assigned to the vibration in the PO_4^{3-} and OH groups of the hydroxyapatite (HA) [58]. The presence of these IR signals in the nanocomposites spectra suggests a hydroxyapatite crystal formation in the mesoporous structure. In the spectra of coumarin thiourea, Fig. 7A(e) and B(c), the characteristic stretching vibration peaks are 3348 cm^{-1} NH, 1687 cm^{-1} C=O, 1301 cm^{-1} N–CS–N, 1258 cm^{-1} C–O, 1449 cm^{-1} C–H deformation of CH_3 group (asymmetric) and 1378 cm^{-1} C–H deformation of CH_2 group (symmetric) vibrations [51]. The presence of coumarin thiourea (I–IV) in the MCM-41, MCM-41-HA and MCM-41-GNRs was confirmed by FTIR (Fig. 7A(b), A(d) and B(b)). The bands at 3348 cm^{-1} , 1687 cm^{-1} , 1449 cm^{-1} , 1378 cm^{-1} and 1301 cm^{-1} are attributed to the presence of coumarin thiourea (I–IV) in the mesoporous structure. Furthermore, the intensities of OH groups absorption at 3400 cm^{-1} and Si–OH at 960 cm^{-1} are reduced significantly after coumarin thiourea (I–IV)-loading.

3.2. Coumarin derivatives (I–IV) release studies

The release kinetics of the coumarin derivatives (I–IV) were studied for both systems over 265 h as shown in Fig. 8. It was observed that the loaded samples did not show a sharp initial burst release during the early stage. The initial burst is attributed to the immediate dissolution and release of the portion of coumarin derivative located on and near the surface of the disks. This system presents a small rate of release up to 10 h of assay, followed by a rather constant release over the subsequent hours. This fact is pos-

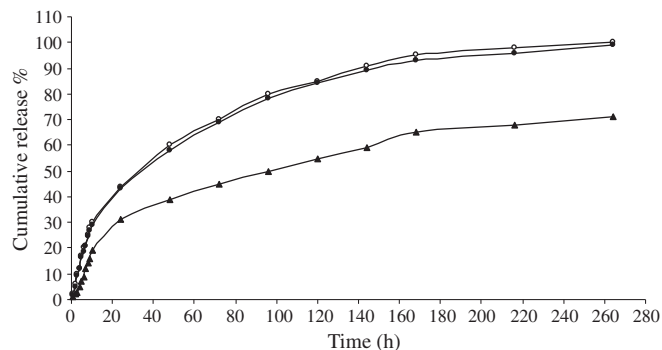


Fig. 8. Sample I release profiles from (●) MCM-41, (▲) MCM-41-HA and (○) MCM-41-GNRs.

sibly related to an interaction between drugs and the mesoporous silica by hydrogen bonding due the affinity of the functional amide group of molecules of coumarin thiourea derivatives and the silanol groups present on mesoporous silica. It was observed that MCM-41-HA system presents a faster release rate during the first 10 h of assays, releasing around 19% of the incorporated coumarin derivatives (I–IV). After that, it presents a slower rate, showing an accumulative release of approximately 70% after 265 h of assays.

The release of coumarin thiourea derivatives (I–IV) from different matrices follows a diffusion-controlled mechanism according to Higuchi model [59] in which the quantity released per unit area is proportional to square root of time. The mechanisms of release from different matrices include the leaching of the coumarin derivatives to the immersion fluid, which can enter the coumarin derivatives-matrix phase through the pores. The drug is presumed to dissolve slowly into the fluid phase and to diffuse from the system along the solvent-filled capillary channels. However, the MCM-41 and MCM-41-HA matrices display a two-step release as shown in Fig. 9. The deviation from overall linearity is probably related to different dissolution rates of the silica matrices. A straight line in the Higuchi plot would correspond to a pure Higuchi type of diffusion-driven release for a carrier where no alteration of the matrix occurs on the time-scale of the release.

The kinetic rate constants (k in h^{-1}) were evaluated and tabulated in Table 2. The k values decreased after the inclusion of hydroxyapatite onto the network of MCM-41. This shows that the HA phase acted as a temporary barrier and prevented the rapid release of coumarin derivatives during assays. Other factors may possibly be related to an interaction between the compounds and the silica mesoporous. Coumarin derivative (I–IV) molecules contain thioamide groups that can interact with silica silanol groups by hydrogen bonding. It was observed that the presence

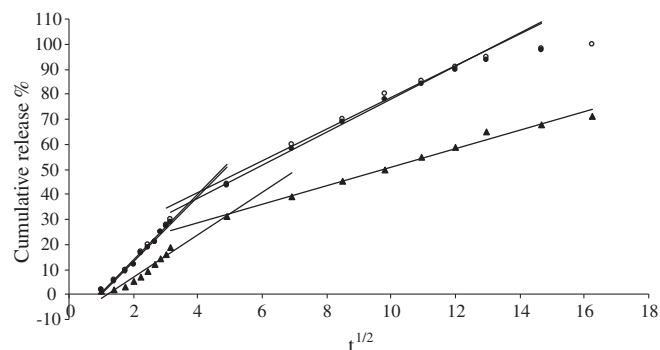


Fig. 9. Higuchi square root of time plots for the release of sample I from (●) MCM-41, (▲) MCM-41-HA and (○) MCM-41-GNRs.

Table 2

Rate constants (k in $\text{h}^{-1/2}$) for first and second stages of coumarin derivatives release from MCM-41, MCM-41-HA and MCM-41-GNRs.

Sample	Stage	k ($\text{h}^{-1/2}$)	r	SD
I MCM-41	First	13.2	0.989	1.062
	Second	6.3	0.990	1.997
MCM-41-HA	First	8.5	0.929	1.759
	Second	3.7	0.986	1.742
II MCM-41	First	13.6	0.989	1.039
	Second	6.3	0.984	2.510
MCM-41-HA	First	8.8	0.938	1.717
	Second	3.9	0.996	0.883
III MCM-41	First	16.4	0.984	1.584
	Second	5.3	0.978	2.512
MCM-41-HA	First	8.8	0.957	1.378
	Second	3.8	0.993	1.221
IV MCM-41	First	16.8	0.982	1.708
	Second	5.9	0.976	2.924
MCM-41-HA	First	9.5	0.929	1.986
	Second	3.9	0.982	2.119
I MCM-41-GNRs	First	13.1	0.991	1.088
	Second	5.7	0.971	2.001
MCM-41-GNRs irradiated at 807 nm For 5 hrs		16.7	0.966	0.801

of HA in the silica matrix played an important role in affecting the percent release from the mesoporous sample. This was ascribed to the apparent interactions between drug/silica/apatite. In silica/apatite system, atenolol can interact with calcium species from HA and silanol groups from silica phase, and this fact can promote a reduction in a delivery rate, depending where the drug is linked [17,60]. A second possibility suggests that an apatite layer precipitated on the surface of nanocomposite can block the pore opening and slow down the release of coumarin derivatives (I–IV). For both MCM-41 and MCM-41-GNRs samples, the early release stages account for about 29% of loaded coumarin derivative (I). The two samples have nearly the same release rate constant (13.2 and $13.1 \text{ h}^{-1/2}$ for MCM-41 and MCM-41-GNRs respectively; Fig. 8).

Gold nanorods of suitable aspect ratios (length divided by width) absorb near infrared (NIR) photons that are a form of heat. Fig. 3 shows TEM image of GNRs. It can be seen that the GNRs have an average aspect ratio of 4.0 with length of ca. 50 nm and width of ca. 12 nm. Fig. 4 shows surface plasmon absorption spectrum of GNRs. The strong long wavelength band in the near infrared region around 800 nm is due to the longitudinal oscillation of electrons. Upon irradiation of MCM-41-GNRs loaded with coumarin derivative (I) at 807 nm, gold nanorods absorb near infrared (NIR) photons and the mechanical fluctuations of the particle ultimately transfer energy to the medium around the particle in a period from 100 ps to 10 ns, depending on the particle size, the medium and pulse energy. The transfer of energy to the medium depends on the thermal conductivity of particles and the medium, the heat capacity of the two, and possibly on solvent viscosity. At this point, the particle has recovered its ground state and has re-attained thermal equilibrium with the medium [61]. This leads to temperature increase. Consequently, there is an increase in release by about 47.6% during the early 5 h. The enhancement ratio of 47.6% was calculated as the ratio of the amounts of release of irradiated and nonirradiated samples. This is attributed to hyperthermia effect of gold nanorods absorbing NIR photons (Figs 10 and 11).

During the first stage of release from MCM-41, bulky cyclohexyl and phenyl derivatives have higher release rates compared with smaller size groups (ethyl and allyl groups). In the second stage,

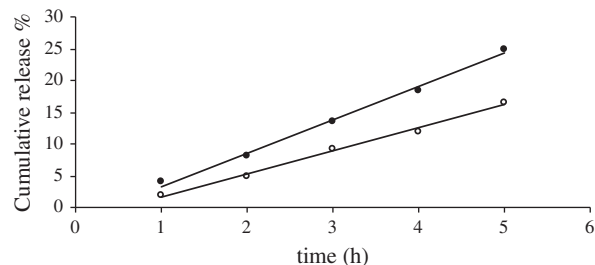


Fig. 10. The early 5 h of sample I release from (○) MCM-41-GNRs and (●) MCM-41-GNRs irradiated at 807 nm using a diode laser source.

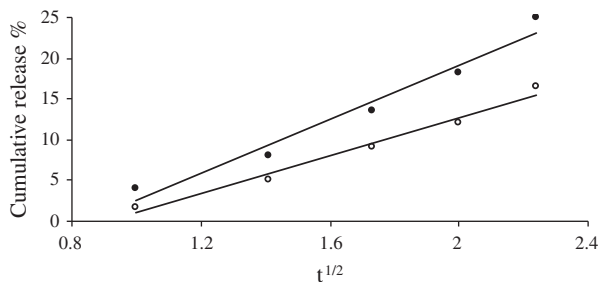


Fig. 11. Higuchi square root of time plot for the early 5 h of sample I release from (○) MCM-41-GNRs and (●) MCM-41-GNRs irradiated at 807 nm using a diode laser source.

release rates are reversed and the release of smaller group derivatives becomes slightly faster (Table 2).

In case of release from MCM-41-HA, the four studied derivatives have nearly the same release rate constant values, and no steric effect was characterized. The existence of two release stages with the early stage faster than the second may be explained in terms of different adsorption locations. The early stage accounts for the release of coumarin molecules adsorbed on the outer surface of mesoporous silicate particles. This accounts for about 30% of loaded samples. This portion of loaded molecules is labile and more bulky coumarin derivatives ($R = \text{cyclohexyl}$ and phenyl ; $k = 16.4$ and $16.8 \text{ h}^{-1/2}$, respectively) are released faster than smaller ones ($R = \text{ethyl}$ and allyl ; $k = 13.2$ and $13.6 \text{ h}^{-1/2}$ respectively). This may be attributed to a less physical contact between thioamide groups of coumarin thiourea derivatives and the silanol groups on silicate particle surfaces leading to less efficient hydrogen bonding.

The second stage of release is slow and accounts for about 70% of loaded coumarin derivatives. This stage accounts for coumarin molecules occupying mesopores of the silicate particles. The release of these molecules is a diffusion-controlled process in which bulky hexyl and phenyl derivatives exhibit slightly less diffusion rate constants (ca. $6.3 \text{ h}^{-1/2}$) compared with less bulky ethyl and allyl derivatives ($k = 5.3$ and $5.9 \text{ h}^{-1/2}$ respectively).

4. Conclusions

The applicability of mesoporous silica MCM-41 and MCM-41-HA materials as matrices for the controlled release was studied for coumarin thiourea derivatives in which the thiourea moiety is linked to functional groups of varying sizes. An effort is made to correlate group size and release rate constants and to establish the influence of the pore architecture and size on the coumarin thiourea derivatives release. The results indicated that mesoporous silica is a potential carrier for encapsulating coumarin derivatives. The incorporation of HA phase in the mesoporous silica led to a

significant change in the structure properties of this system, indicating that incorporation of HA blocks spaces of the mesoporous silica. HA incorporation leads to a decrease in surface area and pore volume with subsequent reduction in release rate constants. Two release stages are also observed. The early release stages account for about 30% of loaded molecules. The presence of HA either on outer surface of silicate particles or inside their mesopores makes a leveling of the release rate constants of the four coumarin derivatives regardless of their size. This may be explained in terms of a more tight binding caused by HA. Unlike HA, loading MCM-41 with gold nanorods does not affect the release kinetics. Only when these samples are irradiated with NIR photons, does the release occur with enhanced rates. This property could be valuable in selected targeting of drugs.

References

- [1] R. Langer, Selected advances in drug delivery and tissue engineering, *J. Controlled Release* 62 (1999) 7–11.
- [2] F. Marcucci, F. Lefoulon, Active targeting with particulate drug carriers in tumor therapy: fundamentals and recent progress, *Drug Discovery Today* 9 (2004) 219–228.
- [3] Y. Shin, J.H. Chang, J. Liu, R. Williford, Y.K. Shin, G.J. Exarhos, Hybrid nanogels for sustainable positive thermosensitive drug release, *J. Controlled Release* 73 (2001) 1–6.
- [4] M. Itokazu, W. Yang, T. Aoki, A. Ohara, N. Kato, Synthesis of antibiotic-loaded interporous hydroxyapatite blocks by vacuum method and in vitro drug release testing, *Biomaterials* 19 (1998) 817–819.
- [5] A. Almirall, G. Larrecq, J.A. Delgado, S. Martinez, J.A. Planell, M.P. Ginebra, Fabrication of low temperature macroporous hydroxyapatite scaffolds by foaming and hydrolysis of an α -TCP paste, *Biomaterials* 25 (2004) 3671–3680.
- [6] J.E. Barralet, K.J. Lilley, L.M. Grover, D.F. Farrar, C. Ansell, U. Gbureck, Cements from nanocrystalline hydroxyapatite, *J. Mater. Sci. Mater. Med.* 15 (2004) 407–411.
- [7] J.A. Jansen, J.G.C. Wolke, E.M. Ooms, Biological behavior of injectable calcium-phosphate (CaP) cement, *Mater. Sci. Forum.* 426 (2003) 3085–3090.
- [8] R.P. Real, J.G.C. Wolke, M. Vallet-Regi, A new method to produce macropores in calcium-phosphate cements, *Biomaterials* 23 (2002) 3673–3680.
- [9] M. Bohner, Calcium orthophosphates in medicine: from ceramics to calcium-phosphate cements, *Injury* 31 (2000) S37–S47.
- [10] J. Karaycki, Monolithic xero-and-aerogels for gel-glass processes, in: L.L. Hench, D.R. Ulrich (Eds.), *Ultrastructural Processing of Ceramics, Glasses and Composites*, Wiley Interscience, New York, 1984, pp. 27–42.
- [11] H.H. Yang, Q.Z. Zhu, H.Y. Qu, X.L. Chen, M.T. Din, J.G. Xu, Flow injection fluorescence immunoassay for gentamicin using sol-gel-derived mesoporous biomaterial, *Anal. Biochem.* 308 (2002) 71–76.
- [12] P. Calicci, S. Salmaso, A. Lante, M. Yoshida, R. Katakai, F. Martellini, I.H. Mei, M. Carenza, Controlled release of biomolecules from temperature-sensitive hydrogels prepared by radiation polymerization, *J. Controlled Release* 75 (2001) 173–181.
- [13] M. Changez, K. Burugapalli, V. Koul, V. Choudhary, The effect of composition of poly(acrylic acid)-gelatin hydrogel on gentamicin sulphate release: in vitro, *Biomaterials* 24 (2003) 527–536.
- [14] T.G.F. Sousa Andreza Sousa, V.V. Silva, L. Botelho, E.M.B. Sousa, SBA15-collagen hybrid material for drug delivery applications, *J. Non-Cryst. Solid* 352 (2006) 3496–3501.
- [15] J.Y. Ying, C.P. Mehnert, M.S. Wong, Synthesis and applications of supramolecular-templated mesoporous materials, *Angew Chem. Int. Ed.* 38 (1999) 57–77.
- [16] G.J.D.A. Soler-Illia, C. Sanchez, B. Lebeau, J. Patarin, Chemical strategies to design textured materials: from microporous and mesoporous oxides to nanonetworks and hierarchical structures, *Chem. Rev.* 102 (2002) 4093–4138.
- [17] A. Sousa, K.C. Souza, E.M.B. Sousa, Mesoporous silica/apatite nanocomposite: special synthesis route to control local drug delivery, *Acta Biomater.* 4 (2008) 671–679.
- [18] M. Vallet-Regi, A. Ramila, R.P. Real, J. Perez-Pariente, A new property of MCM-41: drug delivery system, *Chem. Mater.* 13 (2001) 308–311.
- [19] P. Yang, Z. Quan, L. Lu, S. Huang, J. Lin, Luminescence functionalization of mesoporous silica with different morphologies and applications as drug delivery systems, *Biomaterials* 29 (2007) 692–702.
- [20] M. Manzano, V. Aina, C.O. Arean, F. Balas, V. Cauda, M. Colilla, M.R. Delgado, M. Vallet-Regi, Studies on MCM-41 mesoporous silica for drug delivery: effect of particle morphology and amine functionalization, *Chem. Eng. J.* 137 (2008) 30–37.
- [21] M. Vallet-Regi, J.C. Doadrio, A.L. Doadrio, I. Izquierdo-Barba, J. Perez-Pariente, Hexagonal ordered mesoporous material as a matrix for the controlled release of amoxicillin, *Solid State Ionics* 172 (2004) 435–439.
- [22] G. Cavallaro, P. Pierro, F.S. Palumbo, F. Festa, L. Pasqua, R. Aiello, Drug delivery devices based on mesoporous silicate, *Drug Delivery* 11 (2004) 41–46.
- [23] M. Lin, H. Wang, S. Meng, W. Zhong, Z. Li, R. Cai, Z. Zhou, Q. Du, Structure and release behavior of PMMA/silica composite drug delivery system, *J. Pharm. Sci.* 96 (2007) 1518–1526.
- [24] R. Mellaerts, R. Mols, J.A.G. Jammaer, C.A. Aerts, P. Annaert, J. Van Humbeeck, G. Van den Mooter, P. Augustijns, J.A. Martens, Increasing the oral bioavailability of the poorly water soluble drug itraconazole with ordered mesoporous silica, *Eur. J. Pharm. Biopharm.* 69 (2008) 223–230.
- [25] L.S. Fonseca, R.P. Silveira, A.M. Deboni, E.V. Benvenuti, T.M. Costa, S.S. Guterres, A.R. Pohlmann, Nanocapsule@xerogel microparticles containing sodium diclofenac: a new strategy to control the release of drugs, *Int. J. Pharm.* 258 (2008) 292–295.
- [26] M. Vallet-Regi, F. Balas, M. Colilla, M. Manzano, Bone-regenerative bioceramic implants with drug and protein controlled delivery capability, *Prog. Solid State Chem.* 36 (2008) 163–191.
- [27] F. Balas, M. Manzano, M. Colilla, M. Vallet-Regi, L-Trp adsorption into silica mesoporous materials to promote bone formation, *Acta Biomater.* 4 (2008) 514–522.
- [28] M. Vallet-Regi, F. Balas, D. Arcos, Mesoporous materials for drug delivery, *Angew Chem. Int. Ed.* 46 (2007) 7548–7558.
- [29] A.M. Schwartzberg, T.Y. Olson, C.E. Talley, J.Z. Zhang, Synthesis, characterization, and tunable optical properties of hollow gold nanospheres, *J. Phys. Chem. B* 110 (2006) 19935–19944.
- [30] I.H. El-Sayed, X. Huang, M.A. El-Sayed, Surface plasmon resonance scattering and absorption of anti-EGFR antibody conjugated gold nanoparticles in cancer diagnostics: applications in oral cancer, *Nano Lett.* 5 (2005) 829–834.
- [31] C. Loo, A. Lin, L. Hirsch, M.L. Lee, J. Barton, N. Halas, J. West, R. Drezek, Nanoshell-enabled photonics-based imaging and therapy of cancer, *Technol. Cancer Res. Treat.* 3 (2004) 33–40.
- [32] S.M. Marinakos, S.H. Chen, A. Chilkoti, Plasmonic detection of a model analyte in serum by a gold nanorod sensor, *Anal. Chem.* 79 (2007) 5278–5283.
- [33] J.W. Stone, P.N. Sisco, E.C. Goldsmith, S.C. Baxter, C.J. Murphy, Using gold nanorods to probe cell-induced collagen deformation, *Nano Lett.* 7 (2007) 116–119.
- [34] L.R. Hirsch, R.J. Stafford, J.A. Bankson, S.R. Sershen, B. Rivera, R.E. Price, J.D. Hazle, N.J. Halas, J.L. West, Nanoshell-mediated near infrared thermal therapy of tumors under MR guidance, *Proc. Natl. Acad. Sci. USA* 100 (2003) 13549–13554.
- [35] D.P. O'Neal, L.R. Hirsch, N.J. Halas, J.D. Payne, J. L. West, Photo-thermal tumor ablation in mice using near infrared-absorbing nanoparticles, *Cancer Lett.* 209 (2004) 171–176.
- [36] X.J. Ji, R.P. Shao, A.M. Elliott, R.J. Stafford, E. Esparza-Coss, J.A. Bankson, G. Liang, Z.P. Luo, K. Park, J.T. Markert, C. Li, Bifunctional gold nanoshells with a superparamagnetic iron oxide-silica core suitable for both MR imaging and photothermal therapy, *J. Phys. Chem. C* 111 (2007) 6245–6251.
- [37] X. Huang, I.H. El-Sayed, M.A. El-Sayed, Cancer cell imaging and photothermal therapy in the near-infrared region by using gold nanorods, *J. Am. Chem. Soc.* 128 (2006) 2115–2120.
- [38] B.M.I. Van Der Zande, M.R. Boehmer, L.G.J. Fokkink, C. Schoenenberger, Colloidal dispersions of gold rods: synthesis and optical properties, *Langmuir* 16 (2000) 451–458.
- [39] C.J. Murphy, N.R. Jana, Controlling the aspect ratio of inorganic nanorods and nanowires, *Adv. Mater.* 14 (2002) 80–82.
- [40] B. Nikoobakht, M.A. El-Sayed, Preparation and growth mechanism of gold nanorods (NRs) using seed-mediated growth method, *Chem. Mater.* 15 (2003) 1957–1962.
- [41] J. Lowenthal, H. Birnbaum, Vitamin K and coumarin anticoagulants: dependence of anticoagulant effect on inhibition of vitamin K transport, *Science* 164 (1969) 181–183.
- [42] A. Mizuno, M. Takata, Y. Okada, T. Okuyama, H. Nishino, A. Nishino, J. Takayasu, A. Iwashima, Structures of new coumarins and anti-tumor-promoting activity of coumarins from *Angelica edulis*, *Planta Med.* 60 (1994) 333–336.
- [43] G. Bryantseva, I.V. Sokolova, A.B. Tsyrenzhapova, N.I. Selivanov, V.P. Khilya, Y.L. Garadz, Fluorescent characteristics of coumarin photosensitizers, *J. Appl. Spectrosc.* 75 (2008).
- [44] C. Spino, M. Dodier, S. Sotheeswaran, Anti-HIV coumarin from calophyllum seed oil, *Bioorg. Med. Chem. Lett.* 8 (1998) 3475–3478.
- [45] F. Cottigli, G. Loy, D. Garau, C. Floris, M. Caus, R. Pompei, L. Bonsignore, Antimicrobial evaluation of coumarins and flavonoids from the stems of *Daphne gnidium* L., *Phytomedicine* 8 (2001) 302–305.
- [46] K.C. Fylaktakidou, D.J. Hadjipavlou-Litina, K.E. Litinas, D.N. Nicolaides, Natural and synthetic coumarin derivatives with anti-inflammatory/antioxidant activities, *Curr. Pharm. Des.* 10 (2004) 3813–3833.
- [47] R.O.J. Weinzierl, *Mechanisms of Gene Expression*, Imperial College Press, London, 1999.
- [48] P.M. Aguirre, J.B. Cacho, L. Figueira, M. Lopez, J. Garcia, A.C. Velasco, Rapid fluorescence method for screening *Salmonella* spp. from enteric differential agars, *J. Clin. Microbiol.* 28 (1990) 148–149.
- [49] K.E. Beatty, J.C. Liu, F. Xie, D.C. Dieterich, E.M. Schuman, Q. Wang, D.A. Tirrell, Fluorescence visualization of newly synthesized proteins in mammalian cells, *Angew Chem. Int. Ed.* 45 (2006) 7364–7367.
- [50] A.I. Sherman, M.M. Ter-Pogossian, Lymph-node concentration of radioactive colloidal gold following interstitial injection, *Cancer* 6 (1953) 1238–1240; E.E. Connor, J. Mwamuka, A. Gole, C.J. Murphy, M.D. Wyatt, Gold nanoparticles are taken up by human cells but do not cause acute cytotoxicity, *Small* 1 (2005) 325–327.

- [51] M.Y. Ebeid, K.M. Amin, M.M. Hussein, Coumarinyl thiazolines and coumarinyl thiazolidin-4-ones as potential antimicrobial agents, *Egypt J. Pharm. Sci.* 28 (1997) 183–191;
- A.S. Al-Kady, M. Gaber, M.M. Hussein, E.M. Ebeid, Fluorescence enhancement of coumarin thiourea derivatives by Hg²⁺, Ag⁺, and silver nanoparticles, *J. Phys. Chem. A* 113 (2009) 9474–9484.
- [52] T. Kokubo, H. Kushitani, S. Sakka, T. Kitsugi, T. Yamamuro, Solutions able to reproduce in vivo surface-structure changes in bioactive glass-ceramic A-W, *J. Biomed. Mater. Res.* 24 (1990) 721–734.
- [53] J. Andersson, S. Areva, B. Spliethoff, M. Linden, Sol-gel synthesis of a multifunctional hierarchically porous silica/apatite composite, *Biomaterials* 26 (2005) 6827–6834.
- [54] H. Zhu, B. Lee, S. Dai, S.H. Overbury, Coassembly synthesis of ordered mesoporous silica materials containing Au nanoparticles, *Langmuir* 19 (2003) 3974–3980.
- [55] F. Rouquerol, J. Rouquerol, K. Sing, Adsorption by Powders and Porous Solids, Academic Press, London, 1990.
- [56] P.I. Ravikovitch, D. Wei, W.T. Chueh, G.L. Haller, A.V. Neimark, Evaluation of pore structure parameters of MCM-41 catalyst supports and catalysts by means of nitrogen and argon adsorption, *J. Phys. Chem. B* 101 (1997) 3671–3679.
- [57] Z.S. Deng, J.D. Wei, X.S. Xue, J. Wang, L.Y. Chen, Surface modification of silica aerogels dried with 2-methyl-1-propanol in the sub-critical pressure, *J. Porous Mater.* 8 (2001) 37–42.
- [58] I. Rehman, W. Bonfield, Characterization of hydroxyapatite and carbonated apatite by photo acoustic FTIR spectroscopy, *J. Mater. Sci. Mater. Med.* 8 (1997) 1–6.
- [59] T. Higuchi, Mechanism of sustained-action medication. Theoretical analysis of rate of release of solid drugs dispersed in solid matrices, *J. Pharm. Sci.* 52 (1963) 1145–1149.
- [60] W. Kirch, M. Schafer-Korting, T. Axthelm, H. Kohler, E. Mutschler, Interaction of atenolol with furosemide and calcium and aluminum salts, *Clin. Pharmacol. Ther.* 30 (1981) 429–435.
- [61] M. Hu, G.V. Hartland, in: L.M. Liz-Marzan, P.V. Kamat (Eds.), *Nanoscale materials*, Kluwer, Boston, 2003, p. 97.